International Journal of Technology

http://ijtech.eng.ui.ac.id

Research Article

Volume of Fluid Modeling of CO_2-Water Slug Flow in Circular T-junction Microchannel Reactor

Mohammad Fahmi Al Alam[1], Afiq Mohd Laziz[1,2*], Kok Keong Lau[1,2], Muhammad Nawaz[1], Mohd Zaki Zainal Abidin[3], Teguh Ariyanto[4], Jens Denecke[5]

[1]Department of Chemical Engineering, Universiti Teknologi PETRONAS, Bandar Seri Iskandar, 32610, Malaysia

[2]Centre of Carbon Capture, Utilisation and Storage (CCCUS), Institute of Sustainable Energy and Resources, Universiti Teknologi PETRONAS, Bandar Seri Iskandar, 32610, Malaysia

[3]Faculty of Chemical Engineering, Universiti Teknologi MARA Terengganu, Bukit Besi, 23200, Malaysia

[4]Department of Chemical Engineering, Universitas Gadjah Mada, Yogyakarta, 55281, Indonesia

[5]Institute for Thermo-Fluid-Dynamics, Karlsruhe University of Applied Sciences, Karlsruhe, 76133, Germany

*Corresponding author: afiq.laziz@utp.edu.my; Tel.: +6053687634

Abstract: Carbon dioxide (CO_2) plays a central role in various chemical and environmental processes, and process intensification is often needed to improve efficiency. Microchannel reactors are well-suited for such applications because they provide enhanced mass transfer, particularly when slug flow is formed due to their high interfacial area. Computational Fluid Dynamics (CFD) is widely used to investigate slug flow formation and gas-liquid interface dynamics. However, despite extensive studies, few verified and validated models are available for accurately predicting slug flow, especially in horizontal circular T-junction microchannels. This study aims to develop, verify, and validate a reliable computational fluid dynamics model to simulate slug flow formation using the volume of fluid (VOF) method. The use of CO_2-water system provides realistic hydrodynamic behavior relevant for studying CO_2 hydrodynamics inside microchannel reactors. Mesh sensitivity analysis was conducted using seven meshes to ensure mesh independence and computational efficiency. Mesh sizes beyond 370,000 elements showed only minor improvements in prediction accuracy. The model was then validated against experimental data by comparing the bubble length under multiple flowrate conditions, revealing strong agreement with deviations of 3.04%–6.90%. The experimental data showed high reproducibility with an average coefficient of variation of 2.4%, further confirming the model's reliability. This validated model can serve as a foundation for future CO_2 studies on hydrodynamic optimization, such as the generation of flow pattern maps in microchannel reactors.

Keywords: CO_2 utilization; Computational fluid dynamics; Microchannel reactor; Slug flow

1. Introduction

Carbon dioxide (CO_2) Click or tap here to enter text.is widely involved in various chemical and environmental process. Thus, understanding its behavior is important for improving the overall efficiency of CO_2 conversion, CO_2 adsorption, and CO_2 use. Conventional CO_2-liquid processing is commonly performed in bubble column and stirred tank reactors, which rely on bulk mixing and gas-liquid interface renewal (Heidari et al., 2024; Nickel et al., 2024; Muljani et al., 2023). In recent years, the use of microchannel reactors has gained popularity due to their significantly higher surface-area-to-volume ratio, heat rate, and mass transfer performance (Kumar et al., 2025; Khatoon et al., 2023). Microchannel reactors with typical diameters below 1 mm intensify the reaction kinetics, making them suitable not only for CO_2 chemical processing but also CO_2 conversion, CO_2 adsorption and CO_2 utilization (Cui et al., 2025; Mustafa et al., 2020).

The reactor performance in multiphase microchannel systems is strongly affected by the

https://doi.org/10.14716/ijtech.v17i3.8300
Received December 2025; Revised February 2026; Accepted March 2026

flow regime (Etminan et al., 2022; Liu et al., 2022). Different flow regimes produce varying interfacial areas that ultimately determine the mass transfer efficiency, pressure drop, and mixing behavior (Du et al., 2023; Sattari-Najafabadi et al., 2018). Several flow regimes can be formed depending on fluid properties and gas and liquid flowrate ratio, including annular flow, bubbly flow, and slug flow, as illustrated in Figure 1. The formation of flow regimes is also influenced by channel geometry, orientation, wettability, and dimensionless numbers, such as the Reynolds and Capillary numbers (Li et al., 2025b; Momen et al., 2024; Wang, 2023). Among these flow regimes, slug flow is the most favorable pattern for multiphase microchannels (Rae et al., 2022). This flow exhibits an alternating sequence of liquid slug and gas bubble that can maximize interfacial areas and enhance mass transfer, which is critical and highly relevant for CO_2-related processes (Etminan et al., 2021). On the other hand, circular microchannels are suitable for such processes because the wetting and interface curvature conditions are more uniform than those of rectangular microchannels, which have corners (Zhou and Chang, 2019; Santos and Kawaji, 2012). Accordingly, this study focuses on developing CFD models to predict slug flow formation in circular T-junction microchannels.

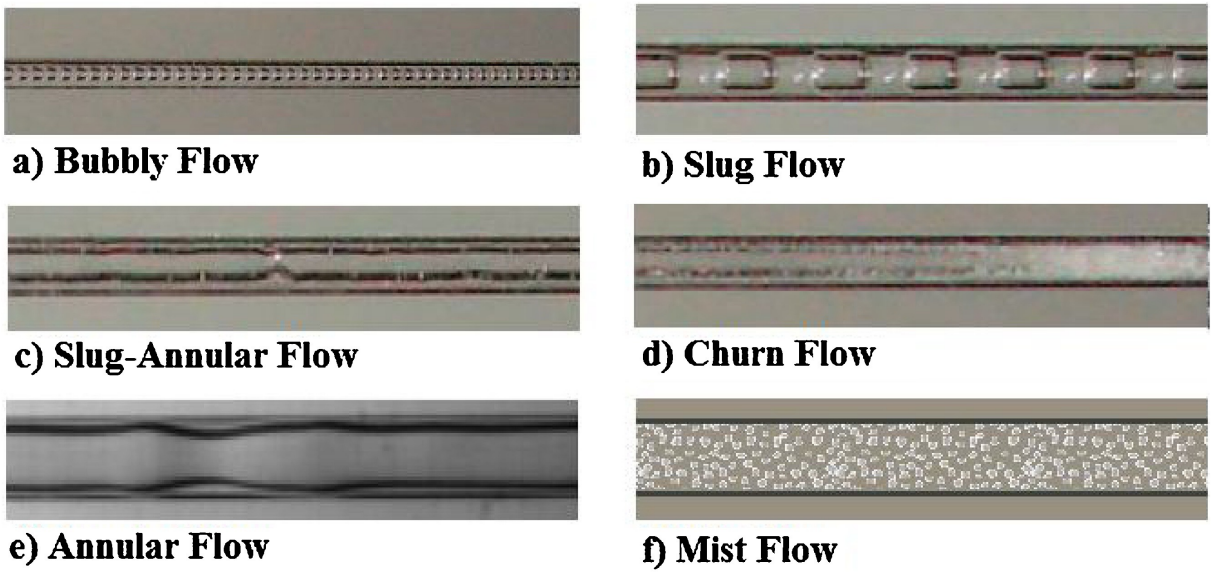

Figure 1 Gas-liquid flow patterns of CO2 inside the microchannel: a) bubbly flow, b) slug flow, c) slug-annular flow, d) churn flow, e) annular flow, and f) mist flow. Reprinted with permission from reference (Sattari-Najafabadi et al., 2018)

CFD is a numerical approach that allows a detailed visualization of slug flow formation and bubble analysis. However, experimental observation can be costly and challenging (Momen et al., 2024; Gao et al., 2022). Among other multiphase modeling methods such as Lagrangian-Eulerian and Euler-Euler, Volume of Fluid (VOF) method has demonstrated superior accuracy for simulating slug flow formation in microchannel reactors (Kim et al., 2024; Ramadan and Park, 2021; Jiang and Zhou, 2020). This is because VOF captures the interface between phases by solving a single set of momentum equations and tracks each phase's volume fraction in every computational cell. Ramadan and Park, 2021 conducted a VOF-based multiphase air-water system in a rectangular T-junction microchannel and achieved an accurate prediction of the bubble length, with the results closely matching those of several benchmark experimental works (Khan et al., 2018; Sobieszuk et al., 2010; van Steijn et al., 2007; Qian and Lawal, 2006). Zhou and Chang, 2019 obtained similar results, where VOF shows reliable prediction of bubble length measurement and interface reconstruction with lower computational cost than the CSLVOF method in a rectangular serpentine microchannel. Gupta and Deshpande, 2023 also confirmed the superiority of VOF in mass conservation and interface tracking. Based on these findings, the VOF method was adopted to model the slug flow formation in this study.

This research aims to develop, verify, and validate a CFD model that incorporates the

VOF method for predicting slug flow formation in a circular T-junction microchannel system using CO_2 and water. While existing research primarily focuses on rectangular microchannels, horizontal circular microchannels remain less explored despite their relevance to practical microchannel reactor design (Ramadan and Park, 2021). Table 1 shows previous key experimental and modeling studies on CO_2 flow regimes in horizontal microchannel. Most prior studies have focused on rectangular or square horizontal microchannels that result in slug, annular, or bubbly flow, whereas only a few studies have explored circular microchannels. Importantly, none of the studies presented a validated CFD model of CO_2-water with circular microchannel that provided both simulation and experimental results, which is covered in this study. The model is validated by comparing the formed bubble length against experimental data under various flow conditions. Mesh sensitivity analysis is incorporated as a verification step to ensure the efficiency of the proposed model.

Table 1 Previous experiments and modeling of CO_2 and horizontal microchannels

Author (Year)	Type of work	Microchannel Profile	Liquid Phase	Flow Pattern
Akkarawatkhoosith et al., 2020	Experiment	Rectangular	Water	Slug-annular, Churn
Janati et al., 2021	Experiment	Circular	MEA + DEA	Annular
Chen et al., 2021	Experiment	Rectangular	[Bmim][BF_4]	Slug
Makarem et al., 2021b	Simulation	Circular	MEA/[Bmim][BF_4]	Slug
Yin et al., 2022	Experiment	Square	ethylene glycol	Slug, Bubbly
Nie et al., 2022	Experiment	Rectangular	[Bmim][BF_4]	Slug, Bubbly
Khatoon et al., 2023	Simulation and Experiment	Rectangular	Water, ethanol, ethyl glycol	Slug, Bubbly
Kurimoto et al., 2024	Simulation	Square	Water	Slug
Mohsin et al., 2025	Experiment	Rectangular	Water	Slug
Jin et al., 2025	Simulation	Rectangular	Water	Slug, Bubbly
Zhu and Zheng, 2025	Simulation	Rectangular	Water	Slug
Cui et al., 2025	Experiment	Rectangular	ZnCe-MOF	Annular

A clear research gap remains in the CFD modeling to predict slug flow formation of CO_2-water system in circular microchannel reactors, as existing CFD validation works are concentrated on air-water system. A second gap arises from the limited number of prior CFD studies using circular microchannels, as the majority uses rectangular microchannels as the working geometry. Accordingly, this study provides a VOF-based CFD model to predict the bubble formation of CO_2-water system in a circular microchannel reactor. The model developed incorporated a comprehensive mesh sensitivity analysis using seven mesh configurations to establish grid independence and identify an optimal balance between accuracy and computational cost. Furthermore, the VOF-based CFD model was validated against experimentally measured bubble lengths across multiple combinations of flow rates, confirming the model's capability for predicting the hydrodynamics inside the microchannel. Therefore, this study establishes a reliable hydrodynamic model that can contribute to future studies on the bubble dynamics of CO_2-water system in circular microchannel reactors, such as generating a flow pattern map.

2. Methodology

This section describes the experimental and computational methods used to develop a reliable CFD model for predicting slug flow formation in a circular T-junction microchannel system using CO_2 and water. Experimental data were obtained to validate the proposed model. Initially, the equipment was calibrated to ensure accuracy and reproducibility before proceeding with the experimental trials. Mesh sensitivity analysis was performed before simulating the system under various flow conditions. The validation criteria aimed to achieve 10% deviation of the average bubble length between the experiment and simulation results.

2.1 Experimental Approach

To validate the developed CFD model, experimental investigations were conducted under controlled flow rate conditions. The experiment focused on analyzing the hydrodynamic behavior of CO_2-water flow inside a circular T-junction microchannel reactor using the bubble length as the key comparison parameter. This metric allows direct comparison with the simulation results. All experiments were conducted at ambient laboratory temperature and atmospheric pressure to ensure consistent fluid properties. Before each measurement, the system was allowed to stabilize for several minutes to eliminate fluctuation in flow rate and bubble formation.

The experimental configuration served as a base for developing the CFD model for accurate validation. Figure 2 illustrates the experimental setup, which consisted of 700 μm main channel and 350 µm perpendicular gas inlet to minimize liquid intrusion into the gas line. The flow rates of the liquid and gas phases were controlled using a calibrated NEW ERA PUMP NE-300 syringe pump and an ASERT AST10-DLCMX mass flow controller operated at ambient temperature and atmospheric pressure, respectively. The bubble formation and flow patterns were observed using an Olympus IX53 inverted microscope equipped with a digital microscope camera. The operations were monitored in real time and captured using the built-in software of the microscope. The bubble was measured from head to tail, and each experimental case was repeated three times with three bubbles measured per trial. The average bubble length of each case was calculated from the mean values of the three trials.

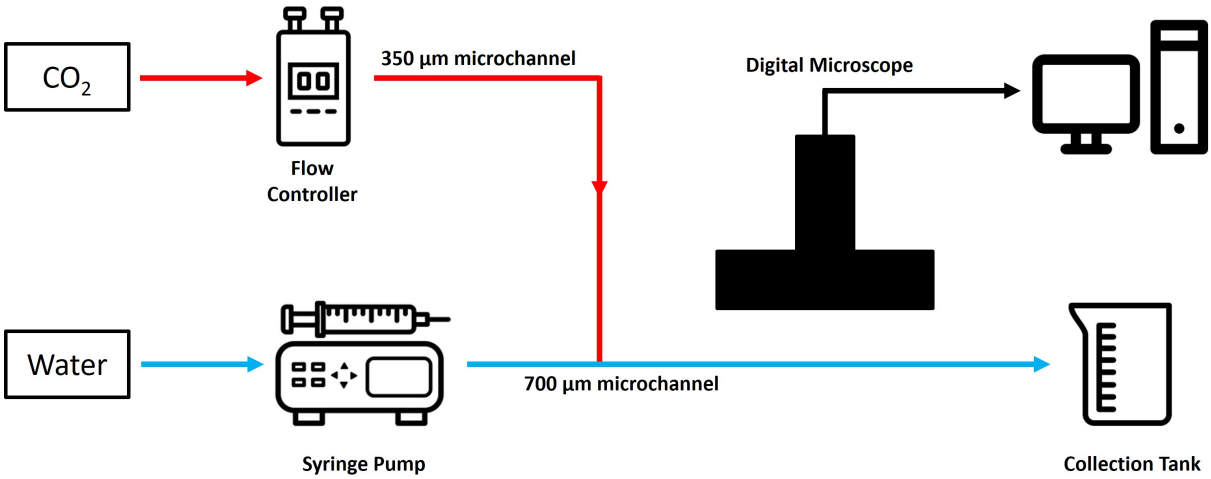

Figure 2 Schematic of the experiment setup

Calibration was performed to ensure accurate flow conditions for both the gas and liquid phases, which is crucial for the simulation and experiment to have similar flow conditions. The set points employed for both phases were within the range of 0.1 mL/min-1.0 mL/min and were repeated three times to confirm reproducibility. Gas calibration used a water displacement technique with the burette to measure CO_2 flow, while liquid calibration was conducted using a gravimetric method that converts collected mass to volumetric flow based on constant density. The resulting gas and liquid calibrations show excellent linearity with R^2 values of 0.995 (Equa-

tion 1; CV 7.81%) and 0.999 (Equation 2; CV 0.89%), respectively, indicating high measurement accuracy. Minor deviations due to equipment backlash and manual reading errors were within acceptable limits.

$$\text{Actual Flowrate} = (0.934 \times \text{Set Point}) - 0.0648 \tag{1}$$

$$\text{Actual Flowrate} = (0.970 \times \text{Set Point}) - 0.0108 \tag{2}$$

2.2 Computational Approach

This study employed CFD using ANSYS Fluent 2023 R2 to predict slug flow formation in a circular T-junction microchannel and replicate the experimental conditions. The VOF model was selected for its ability to capture the interfacial dynamics in a gas-liquid multiphase system. VOF has been widely applied in similar studies and produces high accuracy results in terms of IFB. (Khatoon et al., 2023; Li et al., 2022; Makarem et al., 2021a; Makarem et al., 2021b; Li et al., 2020). The fundamental governing equations used to perform CFD are described as Equation 1 to 4:

The continuity equation for compressible flow is as follows:

$$\frac{\partial \rho}{\partial t} + \frac{\partial (\rho u)}{\partial x} + \frac{\partial (\rho v)}{\partial y} + \frac{\partial (\rho w)}{\partial z} = 0 \tag{3}$$

The continuity equation for incompressible flow is as follows:

$$\frac{\partial (v_x)}{\partial x} + \frac{\partial (v_y)}{\partial y} + \frac{\partial (v_z)}{\partial z} = 0 \tag{4}$$

The momentum conservation law:

$$\rho \left(\frac{\partial \vec{v}}{\partial t} + \vec{v} \cdot \nabla \vec{v} \right) = -\nabla p + \mu \nabla^2 \vec{v} + \vec{F}_x + \rho \vec{g} \tag{5}$$

The energy conservation law:

$$\rho C_p \left(\frac{\partial T}{\partial t} + \vec{v} \cdot \nabla T \right) = \nabla \cdot (k \nabla T) + \Phi \tag{6}$$

2.2.1 Microchannel geometry and domain setup

The microchannel geometry was constructed using CAD software based on the experimental setup. The T-junction consisted of a 700 μm main channel and 350 μm channel placed perpendicularly (Figure 3). The total length of the channel was 12.6 mm, which is 18 times the diameter of the main channel, to ensure sufficient space for the formation of fully developed slug flow. The gas inlet has a length of 1050 μm from the junction point to minimize entrance effects, which can lead to velocity distortion, flow separation, and inaccurate representation of the multiphase pattern (Yan et al., 2024). The outlet boundary is located at the end of the main channel opposite the liquid inlet.

2.2.2 Numerical Setting for Simulating Slug Flow Formation

The incompressible Navier–Stokes equations govern the hydrodynamics of the gas–liquid system and are modeled under transient conditions. A pressure-based solver is used with gravity enabled toward z-axis at -9.81 m/s^2 to replicate the experimental orientation and buoyancy effects. The buoyancy effect is often considered negligible inside the microchannel because of the small scale, where inertial and viscous forces are more dominant. However, a recent study shows that the buoyancy effect still has a significant impact on bubble movement even with a low Bond number (Cranmer et al., 2024). Therefore, this research considers that finding.

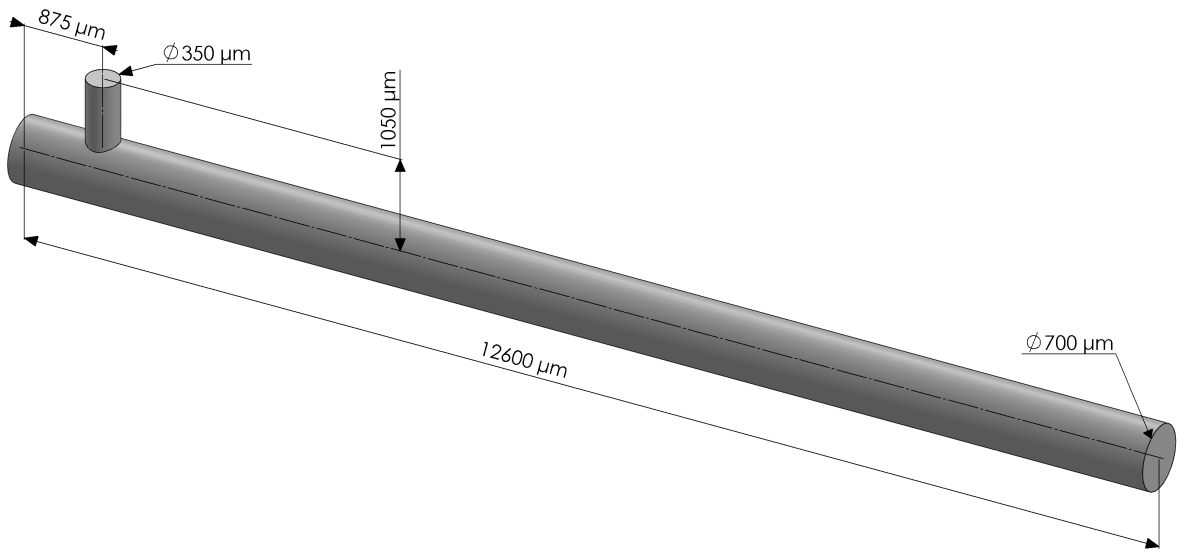

Figure 3 3D geometry of circular T-junction microchannel

The turbulence model used was shear stress transport (SST) k-ω. Although microchannel flows typically exhibit laminar behavior due to small hydraulic diameters and low Reynolds numbers (Re $<$ 1000; Re of this study 15-60), this model can improve prediction accuracy in regions where local inertial effects or interface curvature may induce transitional flow behavior (Miranda et al., 2025). Laminar models cannot accurately replicate phenomena during the squeezing and pinch-off stages of bubble formation. Zhu et al., 2023 demonstrated that SST k-ω provides superior prediction of the shear layer and separation zones compared to other Reynolds-Averaged Navier-Stokes (RANS) models. This model also provides better near-wall resolution and interface sensitivity than standard k–ϵ models, making it suitable for multiphase microchannel simulations involving sharp interface motion and potential shear instabilities (Xu et al., 2022). Kaouachi et al., 2024 further confirmed that in a microscale VOF-based multiphase simulation, SST k-ω proven to be more reliable. During its preliminary simulation, the same study also reported that both the laminar and SST k-ω model produced similar velocity profiles in fully developed regions. However, SST k-ω delivered a more stable and consistent performance during bubble formation. Based on these findings and supported by recent literature, SST k-ω model was adopted in this study.

Additional numerical settings, such as least-squares cell-based gradient reconstruction and warped-face correction, were used to improve the spatial accuracy of polyhedral meshes (Syrakos et al., 2023). These default Fluent options enhance the stability of the solution and are especially relevant for multiphase simulations with strong interfacial curvature (Wang et al., 2019). Tables 2 and 3 show the simulation settings and fluid properties, respectively.

Table 2 Summary of CFD configuration and numerical schemes used in this study

Parameter	Value
Solver type	Pressure-Based
Turbulence model	SST k-ω
Multiphase model	Volume of the fluid
Surface tension modeling	Continuum surface force
Pressure-velocity coupling	SIMPLE
Momentum method	Second-order upwind
Pressure method	PRESTO
Time step size	1×10^{-5}
Courant number	0.25

Table 3 Properties of fluids used in the CFD simulations

Property	CO_2	Water
Density (kg/m^3)	1.79	998.20
Dynamic viscosity (kg/ms)	1.37×10^{-5}	1.003×10^{-5}
Surface tension (N/m)	–	0.072 (Hauner et al., 2017)

2.2.3 Multiphase Modeling Using the VOF

The VOF model is used to capture the interface dynamics between the gas and liquid phases. The volume fraction of each phase is tracked within computational cells and phase interactions are geometrically reconstructed (Guo and Chen, 2009). An explicit formulation with geometric reconstruction is applied to maintain a sharp phase interface. Surface tension is modeled using the CSF method, and wall adhesion is included by specifying a contact angle of 180° at the wall boundary. This configuration represents a non-wetting wall condition, indicating that the liquid will have weak adhesion to the wall geometry. Interfacial anti-diffusion is enabled to prevent numerical diffusion at the interface (Joseph et al., 2019). Equations 7–9 are used to solve the multiphase condition according to Khan et al., 2018.

$$\alpha_L + \alpha_G = 1 \tag{7}$$

$$\rho = \rho_G + (\rho_L - \rho_G)\alpha_L \tag{8}$$

$$\mu = \mu_G + (\mu_L - \mu_G)\alpha_L \tag{9}$$

2.2.4 Boundary Conditions and Cases of Simulation

The simulation includes two velocity inlets and one pressure outlet. The liquid enters the 700 μm main channel, while the gas enters perpendicularly through the 350 μm. The pressure outlet was located at the end of the main channel, with a gauge pressure of 0 Pa. The simulation was performed at 1 atm operating pressure. The domain was initialized with liquid, except for approximately 80% of the gas inlet pre-filled with gas to accelerate convergence. Table 4 Simulation cases used in this study. These parameters were selected because they produced a slug flow, which is the desired flow regime.

Table 4 Operating conditions for 5 cases of CFD simulation

Case	Gas Flow Rate (mL/min)	Water Flow Rate (mL/min)
1	0.40	0.20
2	0.55	0.35
3	0.70	0.35
4	0.70	0.50
5	0.85	0.50

2.2.5 Verifying the Microchannel Mesh for Simulation

The mesh resolution significantly influences the simulation accuracy, as higher resolution yields more precise results. However, a higher mesh density leads to a higher computational cost. Thus, a mesh sensitivity analysis was performed to investigate the most optimal mesh for accurate slug flow formation prediction with minimum simulation cost. Seven different mesh configurations were generated, with maximum cell sizes ranging from 50 μm to 24.5 μm, shown

in Table 5). The simulation was conducted at a gas flow rate of 0.4 mL/min and a liquid flow rate of 0.2 mL/min, as these flow rates correspond to the lowest inlet conditions. Transient time-based simulation was performed until the simulation time reached 0.5 s to ensure the formation of a fully developed slug flow regime.

Table 5 Mesh configuration for the sensitivity analysis

Mesh Setup	Maximum Cell Size (μm)	Number of elements
Mesh 1	50	96,746
Mesh 2	40	172,967
Mesh 3	33	289,976
Mesh 4	30	369,609
Mesh 5	28	449,610
Mesh 6	26	547,902
Mesh 7	24.5	644,523

Figure 4 shows the mesh structure near the junction for mesh 1 (50 μm), mesh 4 (30 μm), and mesh 7 (24.5 μm). As expected, a finer mesh size significantly increases the number of elements and ultimately requires a higher computational cost. Mesh 2 required approximately 20 h to complete the simulation with the available recourse, whereas meshes 4 and 7 required 4 and 7 days, respectively. Further analysis is provided in the Results section.

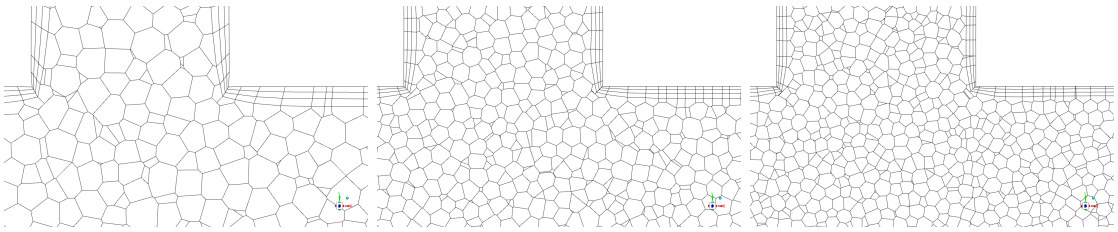

a **b** **c**

Figure 4 Comparison of mesh configurations near the junction: (a) mesh 1 (50 μm, ~97,000); (b) mesh 4 (30 μm, ~370,000); (c) mesh 7 (24.5 μm, ~650,000)

3. Results and Discussion

3.1 Experimental Results and Analysis of CO_2-Water Slug Flow in Microchannels

Table 6 summarizes the results of the experiment. The average bubble length (Mean) produced during the experiments ranged from 1266.7 μm (Case 4) to 1645.9 μm (Case 1). All cases show low variability of bubble formation, indicated by low standard deviation (SD), with the highest occurring in Case 3 (57.1 μm) and the lowest occurring in Case 1 (23.8 μm). The experiments also demonstrated high reproducibility with a CV ranging from 1.4% (Case 1) to 3.6% (Case 3). This result is important for subsequent CFD validation because it confirms the minimal uncertainty in bubble formation. (Ling et al., 2017) used the same approach to validate the drainage and imbibition processes in MPDs. They found that the experimental results were less than 5% in the CV value.

The observed trend strongly agrees with the literature that cases with high gas flow will promote longer bubble length due to gas pressure domination over liquid shear stress at the junction, increasing gas phase penetration into the liquid and delaying pinch-off process by the liquid, and vice versa (Yang and Zhang, 2024). Wang, 2023 also confirmed this finding using a rectangular microchannel, where the bubble characteristic increased from 444 μm to 660 μm as the gas flowrate increased from 30 μL/min to 70 μL/min. Conversely, as the liquid flowrate increases within the same range, the bubble size decreases from 770 μm to 380 μm.

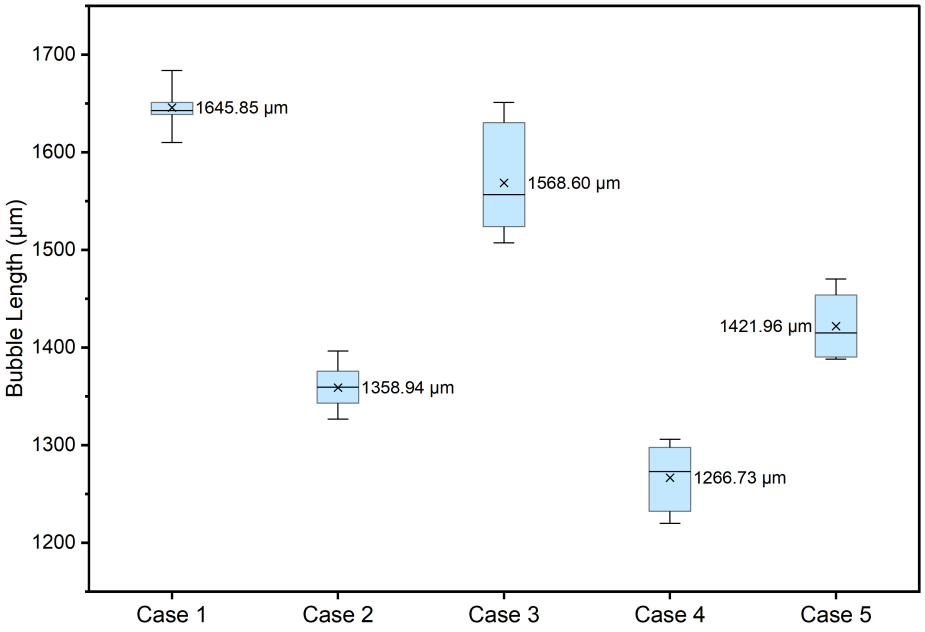

Figure 5 Box and whisker plots of the bubble length (µm) for 5 experiment cases. Boxes show the interquartile range of data (Q1 to Q3), the centerline indicates the median value, and x symbolizes the mean value. CV ranged from 1.44% (Case 1; smaller spread) to 3.64% (Case 3, wider spread)

Table 6 Average bubble length produced during the experiment.

Case	Average Bubble Length (μm)	SD (μm)	CV (%)
Case 1	1645.9	23.8	1.4
Case 2	1358.9	26.2	1.9
Case 3	1568.6	57.1	3.6
Case 4	1266.7	33.1	2.6
Case 5	1422.0	34.2	2.4

3.2 Mesh Sensitivity Analysis for Simulation of Slug Flow

The bubble length was selected as the reference metric for the mesh sensitivity analysis because it is the key hydrodynamic parameter in slug flow that influences the interfacial area and mass transfer. Furthermore, the bubble length formation highly depends on the mesh resolution. Figure 6 reveals a clear trend in the average bubble length formed with increasing number of elements. The results across Mesh 1-7 also generate a power-law trend with R2 of 0.945. A significant decrease in the average bubble size was observed from Mesh 1 to Mesh 2 (15%), followed by smaller variations in subsequent refinements. The difference between Mesh 2 and Mesh 3 is 4% and between Mesh 3 and Mesh 4 is 8%. A noticeable drop of 7% is observed between Mesh 5 and Mesh 6, while only 2% difference is observed between Mesh 6 and Mesh 7. However, the trend shows a slight oscillatory convergence rather than smooth or monotonic convergence. According to Celik et al., 2008 and Roache, 1994, oscillatory convergence in mesh sensitivity analysis is common in multiphase VOF simulation. Their research shows that out of 22 data points, 80% exhibit oscillatory convergence in turbulent flow simulation compared to laminar flow that only occurs on 20% data points. As the mesh resolution increases, small changes in the cell shift the interfacial dynamics during the simulation; in this case, the timing of the bubble pinch-off stage. This phenomenon also occurs when the refinement ratio is below 1.3 (ratio of maximum cell size to the finer mesh's maximum cell size; this research is 1 to 1.25).

This verification process shows that Mesh 4 yields the closest agreement with the experiment (1.57%) despite having less computational process than the finer mesh (Mesh 5-7). Therefore, Mesh 4 (30 μm) was selected as the verified mesh for subsequent validation and simulation studies.

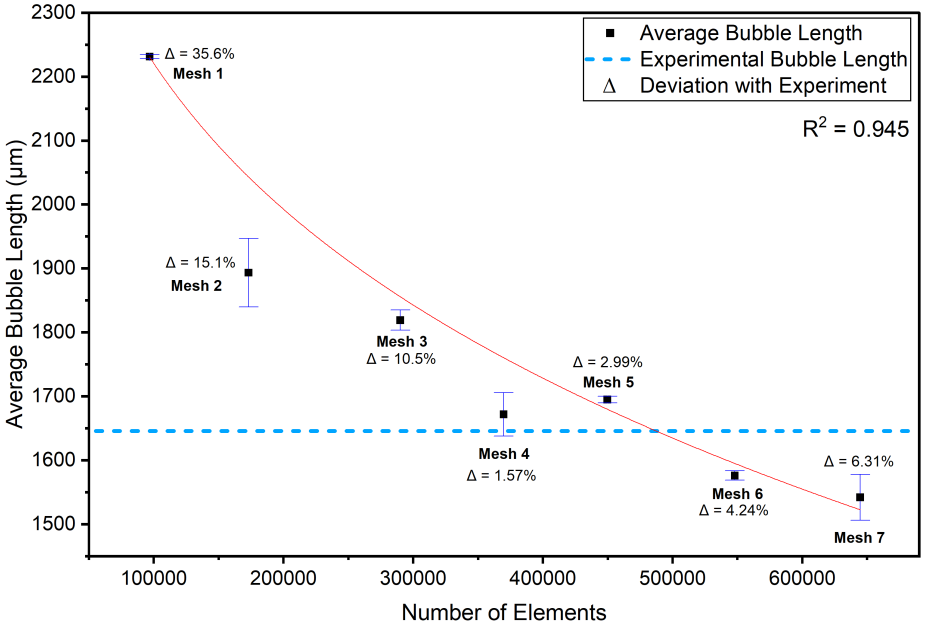

Figure 6 Effect of element counts on bubble size prediction. The bubble length decreases with increasing element count, declining beyond mesh 4 (370,000). Data fitted with a power-law trend ($R^2 = 0.945$). Error bar obtained from 3 bubble data for each mesh configuration

In terms of bubble length accuracy, coarser meshes (Mesh 1-3) show a hug gap of average bubble length compared to experiment while finer mesh (Mesh 4-7) begins to cluster with a relatively small deviation from the experiment (1.5% to 6.3%). Quantitatively, the bubble length deviations from the experiment are 35.6%, 15.1%, and 10.5% for meshes 1–3, respectively. While mesh 4 yielded the closest match (1.6% deviation), meshes 5–7 remained within a 10% deviation range (3.0%, 4.2%, and 6.3%, respectively). Considering both qualitative interface resolution and quantitative deviation, mesh 4 provides the optimal balance between computational cost and accuracy, making it the most suitable for subsequent simulations.

As shown in Figure 7, the bubble shape and length vary noticeably with the mesh size. A clear improvement in consistency is observed from mesh 4 to mesh 7, whereas mesh 1 to 3 produce bubbles with disproportionately thick interfaces compared to finer meshes. The figure shows volume fractions from the simulation results, where a value of 1.0 (red) represents the gas phase, 0.0 (blue) represents the liquid phase, and intermediate colors indicate the diffusion part. The results for meshes 1 to 3 show that coarse meshes with insufficient element resolution cannot accurately capture the thin gas–liquid interface. The diffusion layer is extremely thin; however, in coarse meshes, the interface becomes artificially widened, reducing the accuracy of the result.

This finding aligns with the analysis work of Sadrehaghighi, 2021, who highlighted that mesh sensitivity analysis is crucial for accurate CFD results and that excessive refinements offer negligible accuracy gains. Bargal et al., 2025 also demonstrated similar results in their study using the VOF model to capture Oil-Air interface dynamics in vertical pipe flow. They found an improvement in the interface resolution around the bubbles with mesh refinement but plateaued beyond the number of elements.

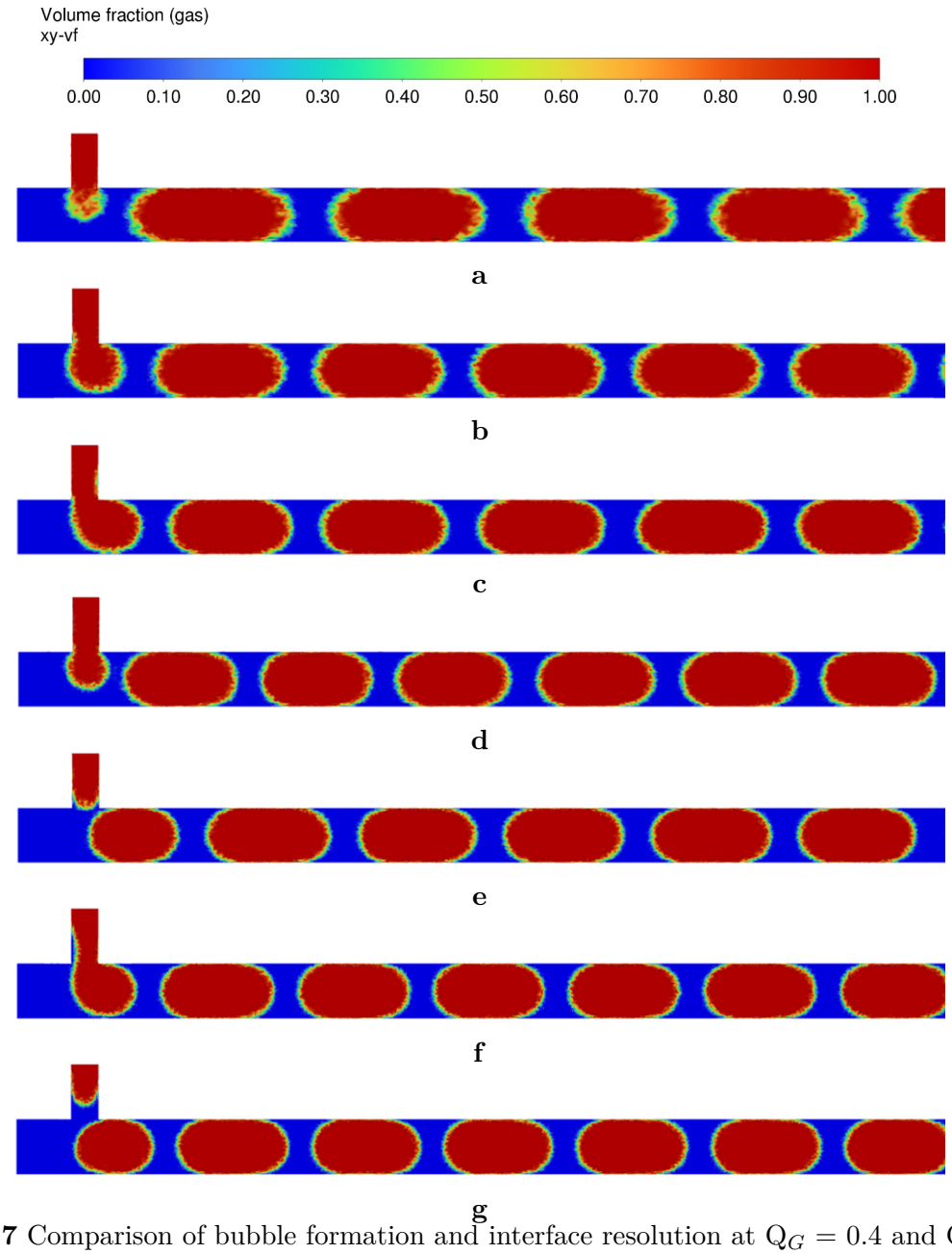

Figure 7 Comparison of bubble formation and interface resolution at $Q_G = 0.4$ and $Q_L = 0.2$ mL/min. Red indicates the gas phase (volume fraction = 1.0), blue indicates the liquid phase (volume fraction = 0.0), and intermediate colors represents gas-liquid interface. (a) mesh 1, (b) mesh 2, (c) mesh 3, (d) mesh 4, (e) mesh 5, (f) mesh 6, and (g) mesh 7

3.3 Comparison of the Average Bubble Length Between the Experiment and Simulation

The bubble length in the slug flow regime is a critical hydrodynamic parameter because it directly determines the interfacial area and mass transfer efficiency. Accurate prediction of bubble length is essential for optimizing flow behavior in microchannel systems dominated by surface force. Thus, the bubble length was selected as the primary validation metric for the CFD model. Figure 8 and Table 7 Comparison of bubble length from simulation and experiment.

The bubble length systematically varied with the flow rate change. The bubble formation began with the gas phase entering the continuous phase (liquid) at the junction, increasing gas-liquid interfacial area. As the bubble expands, it blocks the liquid flow and creates a significant pressure difference. The dominant viscous force then exerts force to squeeze the bubble neck.

Finally, the bubble is pinched off toward the downstream to fully develop its flow, followed by the liquid phase. This mechanism continues to produce alternate bubbles and liquid slugs. Higher liquid flow rates (Case 4 compared to Case 3) produced a shorter bubble length due to the enhanced liquid shear force that promotes earlier pinch-off. Conversely, higher gas flow rates (Case 5 vs. Case 4) generated longer bubbles as more gas accumulated before detachment. This behavior is consistent with the scaling laws proposed by Garstecki et al., 2006, who stated that a higher gas-to-liquid flow rate ratio means longer bubbles in a rectangular microchannel. Although the geometry is cylindrical, the underlying physics of viscous shear and interfacial tension remains consistent. Cylindrical microchannels provide a more uniform interface curvature, resulting in more stable and predictable bubble formation (Zhou and Chang, 2019).

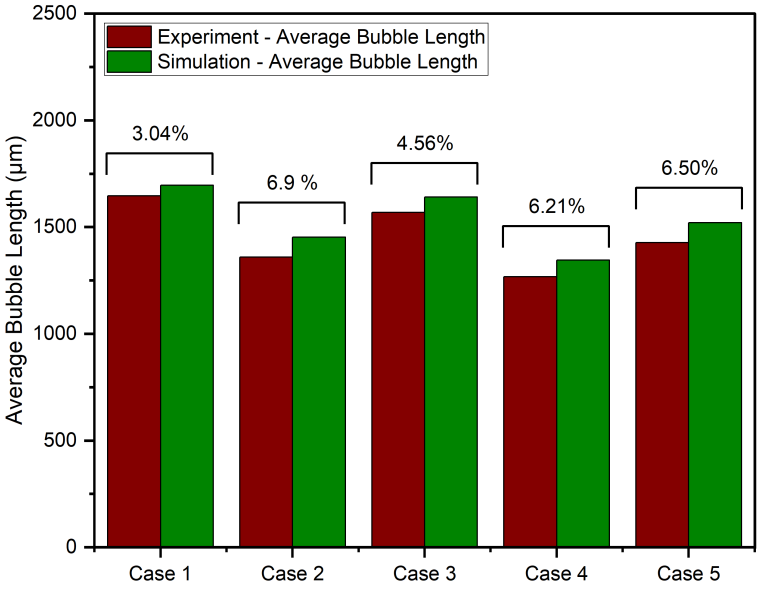

Figure 8 Comparison of the average bubble length between the experiment and simulation across 5 cases. The CFD model replicated all experimental data within a 7% deviation

Table 7 Comparison of the average bubble length between the experiment and simulation.

Case	Average Bubble Length (μm)		Deviation
	Experiment	Simulation	
Case 1	1645.852	1695.883	3.04%
Case 2	1358.937	1452.765	6.90%
Case 3	1568.602	1640.109	4.56%
Case 4	1266.729	1345.375	6.21%
Case 5	1427.319	1520.110	6.50%

The CFD model successfully reproduces these trends, indicating its ability to capture the essential mechanisms of bubble pinch-off processes, such as gas pressure buildup and liquid shear. Habibi Matin and Moghaddam, 2021 reported this transition from capillary-dominated force to shear-dominated breakup. The lowest deviation of the average bubble length between the experimental data and the simulation occurred in Case 1, with 3.04%, while the highest occurred in Case 2, with 6.9%. All cases fall within 7% deviation, confirming the success of the CFD model in accurately predicting bubble length formation. A similar study conducted by Sharaborin et al., 2021 in air-water vertical microchannel system showed a strong agreement of the bubble length between the numerical model and the experiment. Li et al., 2025a also used the bubble length as a key validation metric in air-water system using a rectangular microchannel. Moscato et al., 2025 utilizing liquid-liquid and gas-liquid using a rectangular T-junction microchannel to

achieve a close match between the experiment and simulation using the slug length (liquid-liquid) and bubble length (gas-liquid) as comparative parameters. Wang, 2023 conducted another VOF-based CFD validation work on an air-water system using a rectangular Y-junction microchannel and reported strong agreement with the experiment. The study achieved only 5.4% maximum deviation in bubble length, which is close to the results of this study.

Although the model performs well overall with the experiment, slight deviations in the bubble length may stem from both approaches. The use of a higher-resolution camera could reduce the errors in experimental data extraction. The CFD model prediction can be enhanced by incorporating wetting effects, although this would significantly increase the computational cost.

4. Conclusions

This study developed and validated a VOF-based CFD model for predicting CO_2–water slug flow hydrodynamics in a circular T-junction microchannel. Mesh sensitivity analysis identified Mesh 4 (30 μm, ~370,000 elements) as the optimal configuration, yielding less than a 2% difference from a finer mesh with reduced computational cost. The model was validated against highly reproducible experimental data (average CV= 2.4%) and accurately predicted bubble length across five cases, with deviations ranging from 3.04% to 6.90%. The CFD model successfully captures slug-flow formation, bubble pinch-off mechanisms, and overall hydrodynamic behavior in circular microchannels. From an application perspective, the model provides a reliable foundation for CO_2 hydrodynamic studies in microchannel reactors, including the development of flow-pattern maps to identify operating regimes. Nevertheless, the model does not account for wall wettability or contact-angle effects, which could further enhance predictive accuracy at the expense of increased computational cost, and future work will incorporate high-speed imaging experiments to further refine the model.

Acknowledgements

The authors would like to thank the Chemical Engineering Department at the Universiti Teknologi PETRONAS for their support and contributions to this research and to Yayasan UTP for making this research possible through grant 015LC0-482.

Author Contributions

Mohammad Fahmi Al Alam: Conceptualization, Data curation, Formal analysis, Investigation, Methodology, Software, Validation, Visualization, Writing – original draft. Afiq Mohd Laziz: Funding acquisition, Methodology, Project administration, Resources, Supervision, Validation, Writing – review & editing. Kok Keong Lau: Writing – review & editing. Muhammad Nawaz: Visualization, Writing – review & editing. Mohd Zaki Zainal Abidin: Writing – review & editing. Teguh Ariyanto: Writing – review & editing. Jens Denecke: Writing – review & editing.

Conflict of Interest

The authors declare no conflicts of interest to report regarding this study.

Declaration of AI

During manuscript preparation, the authors used Microsoft Copilot (GPT-5) to check spelling, grammar, clarity, and readability. The authors have carefully reviewed and edited the text and take full responsibility for the final content.

Glossary

α	Volume fraction
C_p	Specific heat capacity
F_{st}	Surface tension force
g	Gravity
k	Thermal conductivity
p	Pressure
ρ	Density
Q_g	Gas volume flow rate
Q_L	Liquid flowrate
Φ	Viscous dissipation
T	Temperature
t	Time
v	Velocity
μ	Viscosity
u	The velocity component in x direction
v	The velocity component in y direction
w	The velocity component in z direction

References

Akkarawatkhoosith, N., Nopcharoenkul, W., Kaewchada, A., & Jaree, A. (2020). Mass transfer correlation and optimization of carbon dioxide capture in a microchannel contactor: A case of CO_2-rich gas. *Energies*, *13*, 5465. https://doi.org/10.3390/en13205465

Bargal, M. H. S., Ben-Mansour, R., Al-Sarkhi, A., & Alhems, L. M. (2025). CFD modeling of two-phase flow (oil/air) with and without rotary mixer inside a vertical pipe for upstream of multiphase pump. *Arabian Journal for Science and Engineering*, *50*, 9611–9630. https://doi.org/10.1007/s13369-024-09789-7

Celik, I., Ghia, U., Roache, P. J., Freitas, C., Coleman, H., & Raad, P. (2008). Procedure for estimation and reporting of uncertainty due to discretization in CFD applications. *Journal of Fluids Engineering*, *130*, 078001. https://doi.org/10.1115/1.2960953

Chen, Y., Zhu, C., Fu, T., & Ma, Y. (2021). Mass transfer enhancement of CO_2 absorption into [Bmim][BF_4] aqueous solution in microchannels by heart-shaped grooves. *Chemical Engineering and Processing: Process Intensification*, *167*, 108536. https://doi.org/10.1016/j.cep.2021.108536

Cranmer, J. A., Sharaborin, E., Khodaparast, S., Giustini, G., & Magnini, M. (2024). Non-negligible buoyancy effect on bubbles travelling in horizontal microchannels of comparable size at small Bond numbers. *International Journal of Multiphase Flow*, *181*, 105019. https://doi.org/10.1016/j.ijmultiphaseflow.2024.105019

Cui, P., Tang, Y., Guo, A., Wang, C., Liu, M., Peng, W., & Yu, F. (2025). Enhanced CO_2 adsorption properties with bimetallic ZnCe-MOF prepared using a microchannel reactor. *Frontiers of Chemical Science and Engineering*, *19*, 14. https://doi.org/10.1007/s11705-025-2518-5

Du, W., Duan, Y., Wang, L., & Liu, D. (2023). Liquid–liquid two-phase flow and size prediction of slug droplets in microchannels. *Processes*, *11*, 2390. https://doi.org/10.3390/pr11082390

Etminan, A., Muzychka, Y. S., & Pope, K. (2021). A review on the hydrodynamics of Taylor flow in microchannels: Experimental and computational studies. *Processes*, *9*, 870. https://doi.org/10.3390/pr9050870

Etminan, A., Muzychka, Y. S., & Pope, K. (2022). Liquid film thickness of two-phase slug flows in capillary microchannels: A review. *Canadian Journal of Chemical Engineering*, *100*, 325–348. https://doi.org/10.1002/cjce.24068

Gao, J., Hu, Z., Yang, Q., Liang, X., & Wu, H. (2022). Fluid flow and heat transfer in microchannel heat sinks: Modelling review and recent progress. *Thermal Science and Engineering Progress*, *29*, 101203. https://doi.org/10.1016/j.tsep.2022.101203

Garstecki, P., Fuerstman, M. J., Stone, H. A., & Whitesides, G. M. (2006). Formation of droplets and bubbles in a microfluidic T-junction: Scaling and mechanism of break-up. *Lab on a Chip*, *6*, 437. https://doi.org/10.1039/b510841a

Guo, F., & Chen, B. (2009). Numerical study on Taylor bubble formation in a micro-channel T-junction using VOF method. *Microgravity Science and Technology*, *21*, 51–58. https://doi.org/10.1007/s12217-009-9146-4

Gupta, R., & Deshpande, A. (2023). CFD modeling of two-phase flow in mini and microchannels. In *Handbook of multiphase flow science and technology* (pp. 1279–1304). Springer. https://doi.org/10.1007/978-981-287-092-6_35

Habibi Matin, M., & Moghaddam, S. (2021). Mechanism of transition from elongated bubbles to wavy-annular regime in flow boiling through microchannels. *International Journal of Heat and Mass Transfer*, *176*, 121464. https://doi.org/10.1016/j.ijheatmasstransfer.2021.121464

Hauner, I. M., Deblais, A., Beattie, J. K., Kellay, H., & Bonn, D. (2017). The dynamic surface tension of water. *Journal of Physical Chemistry Letters*, *8*, 1599–1603. https://doi.org/10.1021/acs.jpclett.7b00267

Heidari, S., Esmaeilzadeh, F., Rafati, R., & Haddad, A. S. (2024). Experimental and modeling of CO_2 absorption in a bubble column using a water-based nanofluid containing co-doped SiO_2 nanoparticles. *Modeling Earth Systems and Environment*, *10*, 3229–3241. https://doi.org/10.1007/s40808-023-01869-1

Janati, S., Aghel, B., & Shadloo, M. S. (2021). Effect of alkanolamine mixtures on CO_2 absorption efficiency in T-shaped microchannel. *Environmental Technology and Innovation*, *24*, 102006. https://doi.org/10.1016/j.eti.2021.102006

Jiang, M., & Zhou, B. (2020). Numerical study of flow regimes in microchannel with dynamic contact angle. *International Journal of Hydrogen Energy*, *45*, 29782–29790. https://doi.org/10.1016/j.ijhydene.2019.09.035

Jin, Z., Liu, Z., Li, Y., Wang, F., & Wang, C. (2025). Impact of contact angle on droplet breakup dynamics in a T-junction microchannel. *Chemical Papers*, *79*, 6315–6332. https://doi.org/10.1007/s11696-025-04193-3

Joseph, M., Mathew, G., Krishnaraj, G., Dilip, D., & Ranjith, S. (2019). Numerical simulation of liquid–gas interface formation in long superhydrophobic microchannels with transverse ribs and grooves. *Experimental and Computational Multiphase Flow*, *2*, 162–173. https://doi.org/10.1007/s42757-019-0043-9

Kaouachi, A., Daoudi, S., & Mahi, I. E. (2024). Effect of turbulence models on multiphase flow through porous media simulation. In *Proceedings of engineering studies* (pp. 227–237). https://doi.org/10.1007/978-3-031-62715-6_13

Khan, W., Chandra, A. K., Kishor, K., Sachan, S., & Alam, M. S. (2018). Slug formation mechanism for air–water system in T-junction microchannel: A numerical investigation. *Chemical Papers*, *72*, 2921–2932. https://doi.org/10.1007/s11696-018-0522-7

Khatoon, B., Hasan, S. U., & Alam, M. S. (2023). CO_2 capturing in cross T-junction microchannel using numerical and experimental approach. *Chemical Papers*, *77*, 6319–6340. https://doi.org/10.1007/s11696-023-02941-x

Kim, S. H., Hong, M. S., & Braatz, R. D. (2024). Investigation of particle flow effects in slug flow crystallization using multiscale computational fluid dynamics simulation. *Chemical Engineering Science*, *297*, 120238. https://doi.org/10.1016/j.ces.2024.120238

Kumar, S., Kumar, P., & Grewal, K. S. (2025). Machine learning-driven multi-objective optimization of microchannel reactors for CO_2 conversion. *Advanced Sustainable Systems*, *9*. https://doi.org/10.1002/adsu.202500064

Kurimoto, R., Hayashi, K., & Tomiyama, A. (2024). Pressure drop and bubble velocity in Taylor flow through square microchannel. *Microfluidics and Nanofluidics*, *28*, 58. https://doi.org/10.1007/s10404-024-02750-y

Li, D., Xing, J., Zhang, Z., & Wang, H. (2025a). Numerical investigation on dynamic behavior of bubbles under forced flow in a microchannel. *RSC Advances*, *15*, 23414–23426. https://doi.org/10.1039/D5RA02116B

Li, Q., Qiao, J., Wang, G., & Chen, S. (2025b). Taylor flow characteristics and mass transfer in curved T-microchannels. *Physics of Fluids*, *37*. https://doi.org/10.1063/5.0252466

Li, W. L., Liang, H. W., Wang, J. H., Shao, L., Chu, G. W., & Xiang, Y. (2022). CFD modeling of CO_2 chemical absorption in a microporous tube-in-tube microchannel reactor. *Fuel*, *327*, 125064. https://doi.org/10.1016/j.fuel.2022.125064

Li, W. L., Wang, J. H., Lu, Y. C., Shao, L., Chu, G. W., & Xiang, Y. (2020). CFD analysis of CO_2 absorption in a microporous tube-in-tube microchannel reactor with novel gas-liquid mass transfer model. *International Journal of Heat and Mass Transfer*, *150*, 119389. https://doi.org/10.1016/j.ijheatmasstransfer.2020.119389

Ling, B., Bao, J., Oostrom, M., Battiato, I., & Tartakovsky, A. M. (2017). Modeling variability in pore-scale multiphase flow experiments. *Advances in Water Resources*, *105*, 29–38. https://doi.org/10.1016/j.advwatres.2017.04.005

Liu, L., Jiang, S., Zhu, C., Ma, Y., & Fu, T. (2022). Distribution of liquid–liquid two-phase flow in branching T-junction microchannels. *Chemical Engineering Journal*, *431*, 133939. https://doi.org/10.1016/j.cej.2021.133939

Makarem, M. A., Farsi, M., & Rahimpour, M. R. (2021a). CFD simulation of CO_2 removal from hydrogen-rich stream in a microchannel. *International Journal of Hydrogen Energy*, *46*, 19749–19757. https://doi.org/10.1016/j.ijhydene.2020.07.221

Makarem, M. A., Kiani, M. R., Farsi, M., & Rahimpour, M. R. (2021b). CFD simulation of CO_2 capture in a microchannel using aqueous MEA and [Bmim]BF_4 with TiO_2 nanoparticles. *International Journal of Thermophysics*, *42*, 1–16. https://doi.org/10.1007/s10765-021-02812-1

Miranda, E. P., Sempértegui-Tapia, D. F., & Chávez, C. A. (2025). Turbulence model performance for predicting fluid flow and heat transfer in micro-scale channels. *Numerical Heat Transfer Part A*, *86*, 4353–4373. https://doi.org/10.1080/10407782.2024.2318001

Mohsin, M., Masood, H. M., Ali, N., Shahzad, K., & Hassan, M. (2025). Hydrodynamic and thermal analysis of water slugs in super-hydrophobic T-junction microchannel. *Journal of the Pakistan Institute of Chemical Engineers*, *52*. https://doi.org/10.54693/piche.05227

Momen, A. M., Sherif, S. A., & Lear, W. E. (2024). Modeling of two-phase gas-liquid slug flows in microchannels. *Computational Thermal Sciences*, *16*, 113–128. https://doi.org/10.1615/ComputThermalScien.2024049784

Moscato, S., Cutuli, E., Camarda, M., & Bucolo, M. (2025). Experimental and numerical study of slug-flow velocity inside microchannels through in situ optical monitoring. *Micromachines*, *16*. https://doi.org/10.3390/mi16050586

Muljani, S., Setyawan, H., & Nugraha, R. E. (2023). Bubble formation in absorber column for CO_2 absorption and precipitated silica production. *RSC Advances*, *13*, 33471–33483. https://doi.org/10.1039/D3RA05860C

Mustafa, A., Lougou, B. G., Shuai, Y., Wang, Z., & Tan, H. (2020). Recent developments in CO_2 utilization for solar fuels and chemicals: A review. *Journal of Energy Chemistry*, *49*, 96–123. https://doi.org/10.1016/j.jechem.2020.01.023

Nickel, N., Fitschen, J., Haase, I., Kuschel, M., Schulz, T. W., Wucherpfennig, T., & Schlüter, M. (2024). Novel sparging strategies to enhance dissolved carbon dioxide stripping in industrial stirred tank reactors. *Frontiers in Chemical Engineering*, *6*. https://doi.org/10.3389/fceng.2024.1470991

Nie, X., Zhu, C., Fu, T., & Ma, Y. (2022). Mass transfer intensification in gas–liquid flow within microchannels with triangular obstacles. *Chinese Journal of Chemical Engineering*, *51*, 100–108. https://doi.org/10.1016/j.cjche.2021.09.016

Qian, D., & Lawal, A. (2006). Numerical study on gas and liquid slugs for Taylor flow in T-junction microchannel. *Chemical Engineering Science*, *61*, 7609–7625. https://doi.org/10.1016/j.ces.2006.08.073

Rae, V. R. S., Laziz, A. M., & Shaari, K. Z. K. (2022). Hydrodynamic study of internal circulation inside microreactor for transesterification process. *IOP Conference Series: Earth and Environmental Science*, *963*, 012018. https://doi.org/10.1088/1755-1315/963/1/012018

Ramadan, Z., & Park, C. W. (2021). Numerical investigation of gas–liquid slug formation in T-junction microchannel using OpenFOAM. *Chemical Papers*, *75*, 4381–4390. https://doi.org/10.1007/s11696-021-01530-0

Roache, P. J. (1994). Perspective: A method for uniform reporting of grid refinement studies. *Journal of Fluids Engineering*, *116*, 405–413. https://doi.org/10.1115/1.2910291

Sadrehaghighi, I. (2021). Mesh sensitivity and mesh independence study. https://doi.org/10.13140/RG.2.2.34847.51365

Santos, R. M., & Kawaji, M. (2012). Developments on wetting effects in microfluidic slug flow. *Chemical Engineering Communications*, *199*, 1626–1641. https://doi.org/10.1080/00986445.2012.660712

Sattari-Najafabadi, M., Nasr Esfahany, M., Wu, Z., & Sundén, B. (2018). Mass transfer between phases in microchannels: A review. *Chemical Engineering and Processing*, *127*, 213–237. https://doi.org/10.1016/j.cep.2018.03.012

Sharaborin, E. L., Rogozin, O. A., & Kasimov, A. R. (2021). Computational study of the dynamics of Taylor bubbles. *Fluids*, *6*, 389. https://doi.org/10.3390/fluids6110389

Sobieszuk, P., Cygański, P., & Pohorecki, R. (2010). Bubble lengths in gas–liquid Taylor flow in microchannels. *Chemical Engineering Research and Design*, *88*, 263–269. https://doi.org/10.1016/j.cherd.2009.07.007

Syrakos, A., Oxtoby, O., de Villiers, E., Varchanis, S., Dimakopoulos, Y., & Tsamopoulos, J. (2023). A unification of least-squares and Green–Gauss gradients under a common projection-based gradient reconstruction framework. *Mathematics and Computers in Simulation*, *205*, 108–141. https://doi.org/10.1016/j.matcom.2022.09.008

van Steijn, V., Kreutzer, M. T., & Kleijn, C. R. (2007). µ-piv study of the formation of segmented flow in microfluidic t-junctions. *Chemical Engineering Science*, *62*, 7505–7514. https://doi.org/10.1016/j.ces.2007.08.068

Wang, L. L. (2023). Study on the effect of gas–liquid two-phase physical features on slug flow in microchannels. *Frontiers in Physics*, *11*. https://doi.org/10.3389/fphy.2023.1125220

Wang, N., Li, M., Ma, R., & Zhang, L. (2019). Accuracy analysis of gradient reconstruction on isotropic unstructured meshes and its effects on inviscid flow simulation. *Advances in Aerodynamics*, *1*. https://doi.org/10.1186/s42774-019-0020-9

Xu, W., Qi, Z., Wang, L., Yang, X., Gao, Q., Huang, L., & Tao, W. (2022). Study of two-phase flow distribution in microchannel heat exchanger header: A numerical simulation. *SSRN Electronic Journal*. https://doi.org/10.2139/ssrn.4054227

Yan, Q., Li, D., Wang, K., & Zheng, G. (2024). Hydrodynamic evolution mechanism and drift flow patterns of pipeline gas–liquid flow. *Processes*, *12*, 695. https://doi.org/10.3390/pr12040695

Yang, G., & Zhang, H.-C. (2024). Investigation of bubble formation dynamics of gas–non-Newtonian liquid two-phase flow in a flow-focusing generator. *Microfluidics and Nanofluidics*, *28*, 63. https://doi.org/10.1007/s10404-024-02757-5

Yin, Y., Chen, W., Wu, C., Zhang, X., Fu, T., Zhu, C., & Ma, Y. (2022). Bubble dynamics and mass transfer enhancement in split-and-recombine (SAR) microreactor with rapid chemical reaction. *Separation and Purification Technology*, *287*, 120573. https://doi.org/10.1016/j.seppur.2022.120573

Zhou, Y. L., & Chang, H. (2019). Numerical simulation of hydrodynamic and heat transfer characteristics of slug flow in serpentine microchannel with various curvature ratio. *Heat and Mass Transfer*, *55*, 3343–3358. https://doi.org/10.1007/s00231-019-02664-4

Zhu, L., Wang, T., Guo, Q., & Yuan, X. (2023). NN-augmented k–ω shear stress transport turbulence model for high-speed flows with shock-wave/boundary layer interaction. *Engineering Applications of Computational Fluid Mechanics*, *17*. https://doi.org/10.1080/19942060.2024.2374316

Zhu, L., & Zheng, L. (2025). Droplet breakup through triangular obstacle in T-junction microchannel. *Physics of Fluids*, *37*. https://doi.org/10.1063/5.0260801